Phosphatidylinositol-Specific Phospholipase C Forms Different Complexes with Monodisperse and Micellar Phosphatidylcholine†

Otto G. Berg,*,‡ Bao-Zhu Yu,§ Rafael J. Apitz-Castro,§ and Mahendra K. Jain*,§

Department of Chemistry and Biochemistry, University of Delaware, Newark, Delaware 19716, and Department of Molecular Evolution, Uppsala University Evolutionary Biology Center, Uppsala, Sweden

Received June 20, 2003; Revised Manuscript Received December 10, 2003

ABSTRACT: Phosphatidylinositol-specific phospholipase C (PI-PLC) from *Bacillus cereus* forms a premicellar complex E# with monodisperse diheptanoylphosphatidylcholine (DC_7PC) that is distinguishable from the E* complex formed with micelles. Results are interpreted with the assumption that in both cases amphiphiles bind to the interfacial binding surface (i-face) of PI-PLC but not to the active site. Isothermal calorimetry and fluorescence titration results for the binding of monodisperse DC_7PC give an apparent dissociation constant of $K_2 = 0.2$ mM with Hill coefficient of 2. The gel-permeation, spectroscopic, and probe partitioning behaviors of E# are distinct from those of the E* complex. The aggregation and partitioning behaviors suggest that the acyl chains in E# but not in E* remain exposed to the aqueous phase. The free (E) and complexed (E# and E*) forms of PI-PLC, each with distinct spectroscopic signatures, readily equilibrate with changing DC_7PC concentration. The underlying equilibria are modeled and their significance for the states of the PI-PLC under monomer kinetic conditions is discussed to suggest that the Michaelis−Menten complex formed with monodisperse DC_7PC is likely to be E#S or its aggregate rather than the classical monodisperse ES complex.

Interfacial enzymes access their substrate from the interface, presumably because their natural substrate is almost exclusively present at organized interfaces of micelles or bilayer (*1*). According to the interfacial kinetic paradigm (*2*−*5*), the enzyme at the interface accesses the substrate through the interfacial binding surface (i-face) in contact with the interface (Figure 1), that is, the interface binding event is different than the catalytic event although the two may be allosterically coupled. The challenge of the interfacial kinetic analysis lies in ascertaining the environment for the microscopic steady-state condition, that is, what the enzyme at the interface "sees" during the processive steady-state turnover. Thus establishing a suitable kinetic assay involves ascertaining (a) the interfacial turnover path and (b) the mole fraction of the active site-directed ligands (L) in the microenvironment of the enzyme at the interface (E*). For a preformed interface, this also requires ascertaining (c) the fraction of the total enzyme in the E* form and (d) how E* is allosterically modulated by the species present in the interface and the aqueous phase. Microscopic processes that also influence the turnover (*1*) include the rate of substrate replenishment, product release, exchange rate of the enzyme between the interfaces, and the allosteric regulation of E*. In effect, structure−function analysis through such kinetic assays requires dissecting the primary events of interest without complications from the competing events. As a step toward such a goal, in this paper we describe an approach toward characterization of the amphiphile interactions along the i-face. The approach is likely to be of general interest for resolution and characterization of the interfacial interactions.

As conceptualized in Figure 1A (*1*−*6*), pre-steady-state binding of an enzyme to the preformed substrate interface is a unique feature for the processive interfacial catalytic turnover by the E* form. Of particular interest for the present study is the possibility that the binding to the i-face of several molecules of a monodisperse amphiphile A that is not an active site directed ligand could form the complex E# as a surrogate or an intermediate for the E* form of the enzyme at the preformed interface. The properties of the half-micellar E# are expected to be different than those of E*. In both E# and E*, the i-face provides the access route to the active site (Figure 1B) and the contacts for the allosteric activation by the interface may or may not be the same in E# and E*. Since the active site directed ligands bind to E, E#, and E* (Figure 1C), at least three distinct kinetic paths could coexist in such a system. We use Figure 1 as a heuristic guide to understand and model (eq 1 in Appendix) interactions of monodisperse and micellar diheptanoyl phosphatidylcholine (DC_7PC)[1] with the i-face of phosphatidylinositol-specific phospholipase C (PI-PLC).

The catalytic behavior of PI-PLC with natural phosphatidylinositol alone in a bilayer or codispersed with phosphatidylcholine is consistent with the interfacial turnover path (*7*−*9*). Crystallographic (*8*, *10*, *11*) and spectroscopic (*7*, *12*, *13*) results suggest that the catalytic site is different than the i-face for the interface binding. The paradigm also accounts for the kinetic behavior of PI-PLC, which catalyzes hydrolysis

† The research was supported by NIH Grant GM-29703 (MKJ) and the Swedish Research Council (OGB).

* To whom correspondence should be addressed. M. K. Jain. Telephone: 302-831-2968. Fax: 302-831-6335. E-mail: mkjain@udel.edu. Otto Berg. E-mail: otto.berg@ebc.uu.se.

‡ Uppsala University Evolutionary Biology Center.

§ University of Delaware.

10.1021/bi035063j CCC: $27.50
Published on Web 01/29/2004

of PI in two steps: the initial formation of 1,2-(cyclic)-inositol phopshate (cIP) by intramolecular phosphotransferase reaction is followed by a phosphodiesterase reaction that converts cIP to inositol-1-phosphate (*9*, *14*, *15*). Apparently, both activities are mediated by the same site, and both steps require the phospholipid interface. PI-PLC also hydrolyzes the micellar PI at a rate that is only 3−10-fold higher than the rate with monodisperse substrate (*9*, *16*, *17*). It has also been reported that the rate of hydrolysis of PI analogues is activated by monodisperse nonsubstrate amphiphile such as phosphatidylcholines (*18*, *19*) with no affinity for the active site (*7*). Since both types of rate increases relate to "activation", it is of interest to discern whether the complex of PI-PLC with the nonsubstrate amphiphiles (A) is a monodisperse EA or EA_2 complex (*18*, *19*) or whether it is a complex $E^{\#}$ (in Figure 1) with several A molecules and thus resembles the interfacial form E*.

In this paper, we compare the properties of E* formed with micellar and $E^{\#}$ formed with monodisperse DC_7PC. Results are consistent with the paradigm in Figure 1 where several DC_7PC molecules bind to the i-face of PI-PLC to form $E^{\#}$. $E^{\#}$ shows propensity for self-aggregation and for the partitioning of hydrophobic solutes. The detailed balance between the E, $E^{\#}$, and E* species (eq 1 in Appendix) is also analyzed to obtain values of the underlying primary equilibrium parameters.

EXPERIMENTAL PROCEDURES

DC_7PC was from Avanti. *N*-Phenyl-naphthylamine (NPN) and *p*-trimethylammonium-diphenylhexatrine (TMA-DPH) were from Molecular Probes. PI-PLC was kindly provided by Dr J. J. Volwerk (*7*). Sources of *N*-dansyl-hexadecyl-1-phosphoethanolamine (HDNS) (*20*) PN14, hexadecyl-phosphocholine (PN16), hexadecyl-1-phosphomethanol (HPM), and octyl-1-phosphomethanol (oct-PM) (*7*) were described before. All measurements were carried out at 24 °C in 10 mM Tris and 20 mM NaCl at pH 8.0. The buffer for size-exclusion chromatography was 20 mM Tris and 0.475 M NaCl at pH 7.4 to minimize the anomalous interactions of the globular proteins with the column matrix (see below).

Critical Micellization and Intermicellization Concentration. Surface tension was monitored by Wilhelmy balance. The critical micellization concentration (CMC) value was determined from the plot of the change in the surface tension of the buffer with the concentration of added amphiphile. The CMC is defined as the minimum amphiphile concentration at which the surface tension of the aqueous phase reaches its minimum. The CMC value obtained in the presence of a fixed concentration of another monodisperse amphiphile in the aqueous phase is called the intermicellar concentration (IMC) for the comicelles. The CMC and IMC values relevant for the present study are summarized in Table 1.

[1] Abbreviations: CMC, critical micellization concentration; DC_7-PC, 1,2-diheptanoylphosphatidylcholine; HDNS, *N*-dansyl-hexadecyl-1-phosphoethanolamine; HPM, hexadecyl-1-phosphomethanol; IMC, intermicellization concentration; MW, apparent molecular weight in kDa; NPN, *N*-phenyl-naphthylamine; oct-PM, octyl-1-phosphomethanol; PI, phosphatidylinositol; PI-PLC, phosphatidylinositol-specific phospholipase C from *Bacillus cereus*; PN16, hexadecylphosphocholine; RET, resonance energy transfer; TMA-DPH, *p*-trimethylammonium-diphenylhexatrine; v_e and v_o, elution and void volumes for size-exclusion chromatography. Abbreviation of the enzyme species and the key parameters are defined in Figure 1 and Appendix.

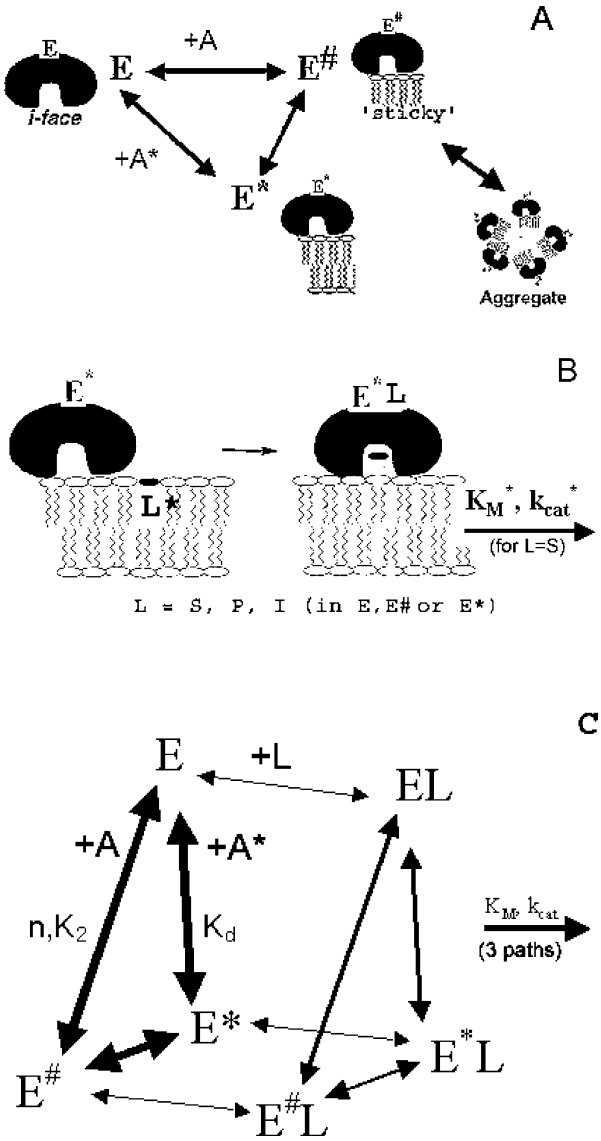

FIGURE 1: Conceptualization of the amphiphile (A or A*) interactions along the i-face of an interfacial enzyme (E). In panel A, E binds to the preformed aggregate A* along its i-face to form E*, or several monodisperse amphiphiles (A) bind to the i-face of E to form $E^{\#}$, which will have propensity to aggregate because the acyl chains of the bound A are exposed to the aqueous phase. Panel B shows binding of active site directed ligand L* (substrate, products, inhibitors) to the active site of E*. In panel C, in the presence of an active site directed ligand L (substrate, product, or inhibitor) each of the enzyme species can form a distinct complex. Catalytic and interfacial binding behaviors of the three complexes describe the microscopic steady-state condition for at least three distinct turnover paths. The focus of the present study is on the equilibria shown by the bold arrows on the left between E, $E^{\#}$, and E* in the absence of L. Results in this paper show that the half-micellar $E^{\#}$ complex of PI-PLC is formed with monodisperse DC_7PC with no significant affinity for the active site of PI-PLC.

Anomalous Retention and Apparent Molecular Weight by Gel Permeation. The conditions and precautions necessary for the size-exclusion chromatography of lipid−protein aggregates of interfacial enzymes were described before (*6*). Larger aggregates show lower elution volume (v_e). Longer retention suggests anomalous interaction of the protein with the column matrix. Most of the size-exclusion results in this paper were obtained on a TSK-250 (250 mm × 7.5 mm) column from Bio-Rad. Some comparisons were also made with the Protein Pack 300 column (Waters). Elution was

Table 1: The CMC and IMC of Amphiphiles

amphiphile	CMC/IMC (mM)
oct-PM	19
DC_7PC	1.5
DC_7PC in 10 mM oct-PM	1.44
DC_7PC in 0.01 mM HPM	0.8−1.4
HPM	0.075
HPM in 1 mM DC_7PC	0.005
HDNS alone	0.01
HDNS in 1mM DC_7PC	0.01
HDNS in 1 μM PI−PLC	0.01
PN14	0.098
PN16	0.009
PN16 in 1 mM DC_7PC	0.004

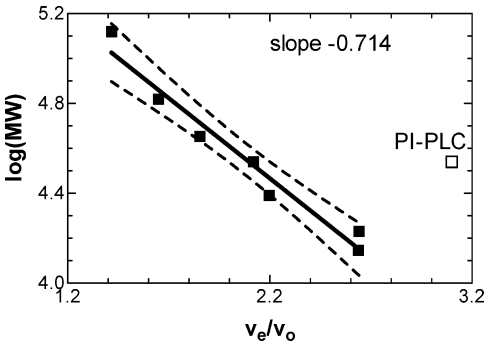

FIGURE 2: Calibration plot of log(MW) versus relative elution volume (v_e/v_o) in 20 mM Tris and 0.475 M NaCl at pH 7.4: (filled symbols from right) pig pancreatic PLA2 (14 kDa), bee venom PLA2 (17 kDa), chymotrypsinogen (24.5 kDa), pepsin (34.7 kDa), ovalbumin (45 kDa), and monomer (66 kDa) and dimer (132 kDa) of bovine serum albumin. The unfilled square to the extreme right marks the retention volume of PI-PLC (MW 34.6 kDa). Retention volume of blue dextran was taken as v_o, which corresponded to the value provided by the manufacturer (obtained with protein aggregate). The slope of the line (with 95% confidence interval shown by dashed lines) corresponds to a 5.18-fold change in log(MW) for a change of 1 in v_e/v_o. Uncertainty of 0.1 min in v_e corresponds to about 10% change in the apparent molecular weight.

monitored on Rainin HPLC system equipped with sequential UV absorbance (at 280 nm) and fluorescence (excitation at 280 nm, emission at 340 nm) detectors with 15 μL flow cells. A comparison of the two outputs is useful to identify potential artifacts, such as the scattering contribution, that interfere with estimation of the protein amounts from the peak area.

The size-exclusion matrix was preequilibrated in the elution buffer without or with the indicated concentration of DC_7PC and other additives. After injection of 6−8 μg of protein in 20 μL of buffer (about 15 μM), the elution rate with the same buffer was kept constant over the next 35−50 min at 1.0 mL/min at 480 psi pressure. The calibration line in Figure 2 shows a near-ideal size-exclusion behavior of the globular proteins that do not interact with the column matrix. This is a necessary condition for obtaining the apparent molecular weight from the calibration curve. Note that the ratio of the elution volume (v_e) to the void volume (v_o) related to the log(MW) is different for different batches of the column from the same manufacturer and significantly different for the columns from different manufacturers.

As shown in Figure 2, the elution volume v_e for 34 kDa PI-PLC is significantly larger than that expected from the calibration standards. Such anomalous retention is attributed to interaction of PI-PLC with the column matrix, and it is independent of the size-exclusion behavior (*6*). For example, with a new Bio-Gel column, the anomalous retention times were reproducible for the first 80−100 runs. In comparison, the size calibration with the noninteracting standards remained acceptable for several hundred runs. Typically, we use the column only until the anomalous retention of PI-PLC and sphingomyelinase did not change noticeably. Such considerations are useful to characterize the size-exclusion behavior of PI-PLC in the presence of monodisperse amphiphiles.

Emission from Intrinsic Fluorescence and the Resonance Energy Transfer. Steady-state fluorescence emission measurements in quartz cuvette were carried out on SLM-Aminco AB2 instrument set in the ratio mode. Slit widths were 4 nm for the emission and excitation wavelengths.

Isothermal Calorimetric Titration. ITC measurements were carried out on the Microcal calorimeter (model VP-itc) with cell volume of 1.42 mL with mechanical stirring at 300 rpm. Standard software was used for the peak integration in relation to the internal calibration. The heat change associated with the dilution of the titrant per injection in the absence of the enzyme was subtracted from the heat change obtained in the presence of PI-PLC. The net heat change per injection in the presence of the enzyme was integrated to obtain the total heat change as a function of the total added amphiphile concentration.

RESULTS

Phosphocholines are neither substrates nor inhibitors of PI-PLC, and therefore, such amphiphiles are ideal surface diluents for the interfacial hydrolysis of phosphatidylinositol by PI-PLC (*7*). On the other hand, alkylphosphomethanols (HPM and oct-PM) are potent competitive inhibitors for the interfacial turnover by PI-PLC. For the inhibition of the hydrolysis of phosphatidylinositol substrate dispersed in phosphatidylcholine bilayer or micelle, 50% inhibition is seen at 0.05 mole fraction HPM. This distinction is useful to analyze interactions of DC_7PC with the i-face of PI-PLC that are characterized in this paper by several methods. Together, these protocols permit analysis of the underlying equilibria between the E, $E^{\#}$, and E* forms (Figure 1).

Micellization. An appreciation of the micellar and intermicellar behavior of amphiphiles is critical to evaluate the conditions for the formation of $E^{\#}$ and E*. According to the standard model of micellization, below its CMC (1.5 mM) virtually all DC_7PC molecules are monodispersed (eq 4). Excess DC_7PC above the CMC is micellar (A*), and the aggregation number is 50−70 up to 5 mM and larger at the higher concentrations (*21*). As summarized in Table 1, the micellization concentration of an amphiphile changes significantly if codispersed with another amphiphile. Such IMC values cannot be predicted from the CMC values of the two amphiphiles. Also the total number of comicelles is limited by the concentration of the limiting amphiphile, as well as by the ratio of the two amphiphiles if they form a stoichiometric molecular complex. Beyond such limits, the mixtures will be a mixture of micelles of differing compositions.

Anomalous Retention of PI-PLC During the Size-Exclusion Chromatography. During electrophoresis on native polyacrylamide gel, as well as with SDS−PAGE, PI-PLC migrates as a single band of 34 kDa. The same value is also

Table 2: Elution Volume (v_e in mL) and the Apparent MW[a] of PI-PLC (34 kDa) Aggregates with Amphiphiles

amphiphiles	v_e and (apparent MW)
void volume v_o	4.96
expected for a 34 kDa protein	9.6
a. PI−PLC (in the buffer only)	14
b. (a) + 3 mM DC_7PC	19 + (>500 kDa)
c. (b) + 10 μM oct-PM	19 + (>500 kDa)
d. (b) + 10 μM HPM	21 + (>500 kDa)
e. (b) + 10 μM PN16	21 + (>500 kDa)
f. (a) + 0.7 mM DC_7PC	17 (main peak) + (220 kDa) + (50 kDa)
g. (f) + 100 μM oct-PM	27 (main peak) + (220 kDa) + (50 kDa)
h. (f) + 10 μM PN16	(>500 kDa) + (250 kDa) + (50 kDa)
i. (a) + 3M urea	14
j. (a) + 100 μM HPM	14
k. (a) + 100 μM PN16	(100 kDa)
l. (a) + 30 μM PN16	(100 kDa) + (50 kDa)
m. (a) + 10 μM PN16	14
n. (a) + 1 μM HDNS	14
o. (n) + 10 μM PN16	14 (broad peak)
p. (a) + <0.5 mM DC7PC	14−30

[a] Elution volumes (v_e) are given for the anomalous peaks that elute later than that expected for a calibration standard of 34 kDa (Figure 2) with ideal size-exclusion behavior.

obtained by mass spectrometry of our preparation. As noted before for the *Listeria* PI-PLC (*22*) and shown in Figure 2, *Bacillus cereus* PI-PLC is retained longer than expected. Its elution volume (v_e = about 14 mL) corresponds to an apparent molecular weight of less than 5 kDa. We believe that this anomalous retention is from the interaction with the hydrophobic patches on the matrix. According to Dr. Donna Hardy of Bio-Rad, the Bio-Sil SEC silica matrix is first sialated and then covalently modified with a diol. Our interpretation is that the modification leaves an uncontrolled distribution of the hydrophobic patches against the background of the diol-modified hydrogen-bonding hydrophilic surface. Since v_e for PI-PLC does not change in the presence of 3 M urea (Table 2, entry i), we assume that the anomalous interactions are not due to specific hydrogen-bonding interactions.

Self-Aggregates of PI-PLC with Micellar and Monodisperse DC_7PC. As summarized in Table 2, PI-PLC elutes in multiple peaks from the column equilibrated with monodisperse and micellar DC_7PC (CMC = 1.5 mM) in the elution buffer. Typically, 6−8 μg of PI-PLC (about 15 μM) injected elutes in peak areas of 1−3 mL, which will correspond to the protein concentration of about 0.1 μM. This precludes analysis of the protein/lipid ratio for the eluted complex in the peak. Also if the complex continuously changes with the dilution on the column, apparent size obtained from the elution volume and the calibration curve will only be a lower limit estimate. Below 0.5 mM monodisperse DC_7PC, PI-PLC is retained longer and elutes as several broad peaks. Such a behavior is consistent with the formation of $E^{\#}$ and its interaction with the matrix along the exposed acyl chains at the i-face. Although very useful as a qualitative diagnosis of $E^{\#}$ formation, from the anomalous elution behavior we cannot tell whether PI-PLC elutes as a complex or whether the complex dissociates during the elution. The elution behavior is also expected to change as the hydrophobic patches partition different amounts of DC_7PC at different concentrations. Such possibilities preclude interpretation of the anomalously retained peaks that elute at all concentrations between 0 and 3 mM DC_7PC in the elution buffer (Table 2). Since these measurements were carried out in the column equilibrated with the indicated concentrations (in the millimolar range) of the lipids, it is not possible to measure the concentration changes associated with the coelution with <10 μM PI-PLC in the elution peak.

Above 0.6 mM DC_7PC, some of the PI-PLC begins to elute with smaller v_e. Apparent molecular weights for such faster eluting peaks are given in Table 2. The elution volume and the relative peak intensities (results not shown) depend on the concentration of DC_7PC and other amphiphiles in the elution buffer. In 3 mM DC_7PC, PI-PLC elutes in two peaks (b) of nearly equal area. The first peak elutes with the front (about 5 mL) corresponding to the apparent MW of >500 kDa. The second peak elutes at 19 mL as if it "sticks" to the matrix more strongly than does PI-PLC alone, as would be expected for $E^{\#}$ complex on a hydrophobic matrix. The elution profile is unchanged in 3 mM DC_7PC with 10 μM oct-PM, HPM, or PN16 (c, d, and e in Table 2), although the shape and position of the anomalously retained peaks change somewhat.

A key result in Table 2 is that in monodisperse (0.7 mM) DC_7PC alone (f), or with 0.1 mM oct-PM (g), PI-PLC also elutes as 220 and 50 kDa aggregates. The anomalous peak is retained longer in the presence of oct-PM. On the other hand, anomalous retention is not seen with comicelles (h) or micelles of PN16 (k, l). The aggregate size also changes with the concentration of PN16 micelles, whereas the aggregates are not formed at the CMC of PN16 (m) or HPM (j).

Apparent sizes of the PI-PLC aggregates are intriguing. Results in Table 2 show that only four aggregates of MW >500, 200, 100, and 50 kDa are formed. For example, a 500 kDa aggregate in micellar DC_7PC (b−e, j−l) implies that the native DC_7PC micelle (20−35 kDa with aggregation number of 50−70) binds several PI-PLC molecules. If so, the 100 kDa aggregate could have 60 DC_7PC molecules with two PI-PLC or 150 DC_7PC molecules with one PI-PLC. In the 50 kDa aggregate with one molecule of PI-PLC, the number of DC_7PC will only be 30. In any case, formation of PI-PLC aggregates with monodisperse DC_7PC rules out formation of simple EA or EA_2 complexes.

Together, the size-exclusion behavior in micellar and monodisperse DC_7PC shows that PI-PLC aggregates of only a few defined sizes are formed. The size estimates are based on the assumption that the eluted aggregate does not interact with the matrix and that the aggregate size does not change during the elution. Whether explicitly stated or not, all estimates of apparent molecular weight by size exclusion are based on this assumption. If anomalous interactions of the faster eluting species with the matrix persist, then the size estimates given in Table 2 are only the lower limit estimates.

Isothermal Calorimetric Titration of PI-PLC with DC_7PC. The monodisperse DC_7PC concentration dependence of the net exothermic enthalpy change for the interaction with 1.7 μM PI-PLC is shown in Figure 3. Two phases are distinguishable. Below the CMC the fit is for a cooperative binding of monodisperse DC_7PC (eq 8b) with $n = 2.1$ and $K_2 = 0.2$ mM. The enthalpy change, determined separately by the titration of 1 mM DC_7PC with PI-PLC, is −50 kcal/mol (with 30% uncertainty). Note that K_2 is an apparent dissociation constant in the Hill equation (eq 8b) and it is not directly

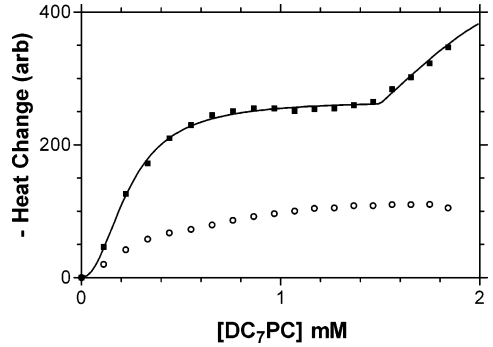

FIGURE 3: Exothermic enthalpy change (in arbitrary units) on the titration with DC_7PC of (○) buffer alone or (■) the net change with 1.7 μM PI-PLC (where the heat of dilution of DC_7PC is already subtracted). The change below the CMC (1.5 mM) is fitted (continuous line) to the Hill equation (eq 8b) with $n = 2.14$ and $K_2 = 0.24$ mM (with 20% uncertainty). Above the CMC, the fit is to eq 8a using the same K_d and N as deduced from Figure 8 with an extra enthalpy contribution from the binding of E and $E^{\#}$ to micelles.

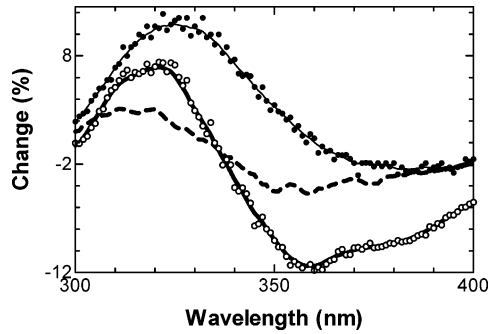

FIGURE 4: Change (% normalized at 338 nm) in the tryptophan fluorescence emission spectrum (excitation 280 nm) of PI-PLC on the addition of 0.4 mM DC_7PC (E to $E^{\#}$) in (− − −) pH 8 buffer with 20 mM NaCl or (○) pH 6.9 buffer with 0.474 M NaCl. These biphasic changes are different than those for E to E* (●) on the addition of 5.5 mM DC_7PC to Pi-PLC in either of the two buffers.

related to the free energy of the underlying interaction. The beginning of the enthalpy change above 1.5 mM DC_7PC in Figure 3 suggests that an additional enthalpy change is associated with the formation of E*.

Tryptophan Spectral Changes in PI-PLC. Characteristic changes in the tryptophan emission spectrum of PI-PLC are observed under a variety of conditions including the presence of organic solvents and functionally relevant additives. At least two types of changes are clearly distinguishable (Figure 4): a biphasic spectral change (with a peak and a trough) occurs on the formation of $E^{\#}$ from E, and only a peak centered at 330 nm is observed in the spectral change associated with the formation of E* from E. The origins of such changes are not assigned. PI-PLC from *Bacillus thuringiensis* and *Bacillus cereus* contain seven tryptophan residues in the same positions, whereas only one (W19) is conserved among the three tryptophan residues in the PI-PLC from *Listeria monocytogenes*. Tryptophan-mutagenesis results on the *B. thuringensis* PI-PLC (*12*, *13*) suggest that the increase at 333 nm induced by micellar DC_7PC is most likely due to the perturbation of the solvent-accessible W47 and W242, possibly part of the i-face (*8*, *10*, *23*). Having noted that, we point out that a difference in the spectral changes associated with the formation of $E^{\#}$ and E* (Figure 4) does not necessarily suggest that different tryptophan residues are involved in the interactions with DC_7PC. The

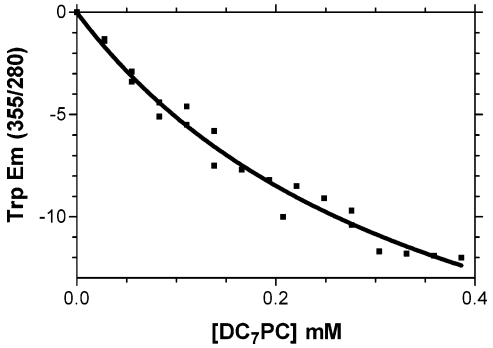

FIGURE 5: The DC_7PC concentration-dependent change in the tryptophan emission intensity at 355 nm (excitation at 280 nm) of PI-PLC (1 μM PI-PLC) in pH 6.9 buffer with 0.474 M NaCl. The fit (continuous line) to the Hill equation (eq 8b) is for $K_2 = 0.11$ mM and $n = 1.72$.

spectral changes could also result from a difference in the internal quenching groups in the vicinity of the same tryptophan residue(s).

Changes in the Tryptophan Emission with Monodisperse DC_7PC. Results in Figure 5 show that a decrease in the emission intensity at 355 nm is induced with monodisperse DC_7PC. The change as a function of DC_7PC concentration is adequately fitted to a Hill equation (eq 8b) with $n = 1.7$ and $K_2 = 0.11$ mM for $E^{\#}$. Considering the noise level in the intensity values, and about 10% overall decrease, we believe that the results are not inconsistent with the calorimetric results given in Figure 3.

Resonance Energy Transfer (RET) Signal from HDNS Bound to E and Partitioned in $E^{\#}$. Insights into the properties of the $E^{\#}$ complex are provided by results in Figure 6A where the RET signal from HDNS increases as it is colocalized in $E^{\#}$ formed in the presence of monodisperse DC_7PC. As shown in Figure 6B, the increase in the RET signal from PI-PLC + HDNS mixture with added DC_7PC is also accompanied by a simultaneous decrease in the signal from the tryptophan donor in PI-PLC. The RET signal (Figure 6A) reaches its maximum at 1 mM and then decreases above 1.5 mM DC_7PC. The rising phase could be due to a combination of at least three factors in relation to the changes in the E + HDNS complex (see below): an increase in the extent of colocalization of HDNS + PI-PLC, an increase in the energy transfer efficiency, or a decrease in the self-quenching. Such changes could also reverse in the falling phase of the RET signal at the higher DC_7PC concentration. At least a large part of the decrease is attributed to the dilution of HDNS from the $E^{\#}$ complex (Figure 6B) into the DC_7PC micelles that begin to form above 1.5 mM. With excess micelles, the residual RET signal is virtually the same as with a mixture of HDNS and micellar DC_7PC without PI-PLC. These results are qualitatively consistent with the model for the formation of $E^{\#}$ (Figure 1).

A quantitative analysis of the results in Figure 6A is hampered by the fact that a significant initial increase in the intensity seen on the mixing of PI-PLC to HDNS (without DC_7PC) suggests formation of a binary complex. This interaction was monitored by two complementary methods. Results in Figure 7 show that the underlying process is rather complex. In Figure 7A, 0.5 μM HDNS is titrated with increasing amount of PI-PLC and monitored as the increase in the RET signal at 500 nm (with excitation at 280 nm). In

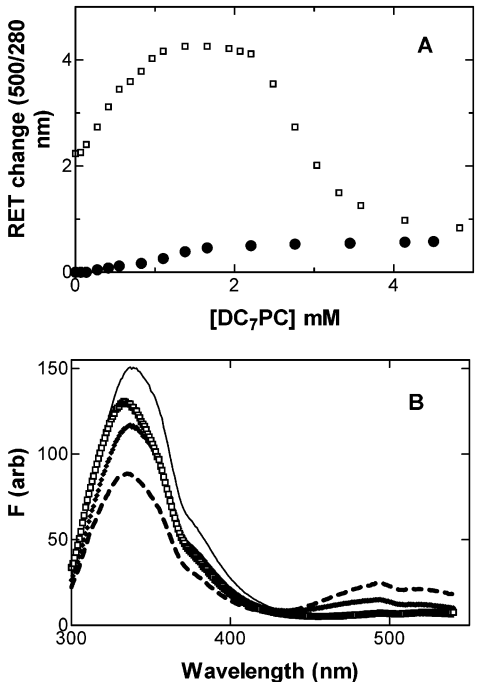

FIGURE 6: Change in the (□) RET signal intensity [A] of 1 μM HDNS (CMC = 10 μM) acceptor at 500 nm (excitation 280 nm) and 1 μM PI-PLC donor on titration with DC_7PC. A control (●) without PI-PLC showed only a small increase (0.5 units on this scale) in the signal at the CMC. Panel B shows the fluorescence emission spectrum (excitation 280 nm) of 1 μM HDNS and 1 μM PI-PLC in the presence of (—) 0, (◆) 0.41, (– – –) 1, and (□) 5.5 mM DC_7PC. Other conditions were the same as thos in panel A.

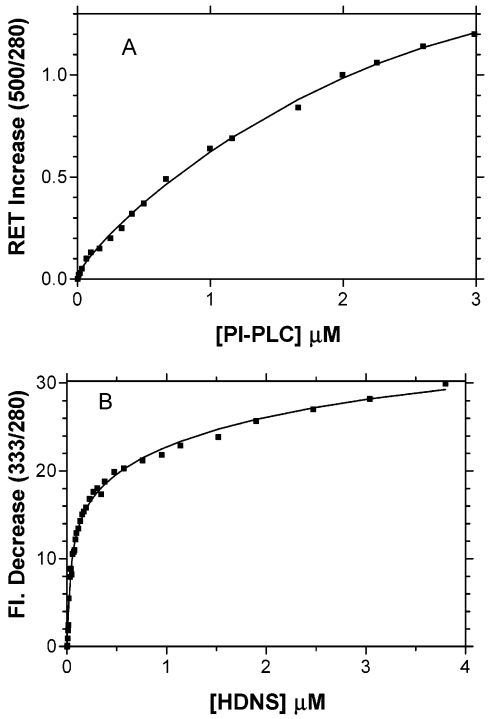

FIGURE 7: Titration of [A] 0.5 μM HDNS (monitored as an increase in the RET signal at 500 nm) with PI-PLC. The best fit shown is for a model (eq 12) where E binds either a single HDNS (K_1 = 0.05 μM) with a strong signal or N_2 = 20−25 HDNS molecules with a very weak signal. This second binding state can be described by Hill parameters n = 5 and K_2 = 0.03 μM. Panel B shows the titration of 0.5 μM PI-PLC (monitored as a decrease in the tryptophan emission at 333 nm) with HDNS. The best fit to eq 12 is with n = 5, N_2 = 25, K_1 = 0.1 μM, and K_2 = 0.03 μM. These numbers are not too different from those in the reverse titration in panel A.

Figure 7B, 0.5 μM PI-PLC is titrated with HDNS, and the signal is for the decrease in the emission at 333 nm from the tryptophan donor. Both of these results show that the underlying process is not necessarily a simple one-step stoichiometric binding of one HDNS to one PI-PLC. The best fits are in a model (section 2 in the Appendix) where the enzyme either binds HDNS singly (with dissociation constant K_1) or binds N_2 = 25 HDNS molecules with Hill parameter n = 5 and dissociation constant K_2. The goodness of fit in Figure 7A or 7B is very insensitive to the choice of N_2 (between 10 and 35), but the choice influences the estimates of the other parameters.

Tryptophan-Signal with PI-PLC on Micelles. As shown in Figure 8, the increase in the tryptophan-emission intensity from PI-PLC (Figure 4) at 333 nm increases sharply at the CMC of DC_7PC. Based on the results in Figure 4, this cannot be interpreted as a lack of interaction of monodisperse DC_7PC with PI-PLC. The change at 333 nm is essentially due to the formation of E*. The data points in Figure 8 are fitted in terms of K_d = 0.76 μM and N = 290 (Appendix, section 1) for the dissociation of E* from micelle to E using n = 2 and K_2 = 0.2 mM. In fact, reasonable fits to these data can be achieved for a range of N between 240 and 330 corresponding to a range of 1.2−0.49 μM for K_d. N is an apparent site-exclusion parameter that accounts for the number of micellar amphiphiles that are removed from further binding for each E* formed. K_d by definition is the dissociation constant from E* to E. The estimate of K_d is very sensitive to the choice of K_2 and n used in the fit for Figure 8. However, with the values of K_2 and n estimated from Figures 3 or 5, virtually all unbound enzyme will be in the $E^{\#}$ form at the CMC. Therefore it follows from the

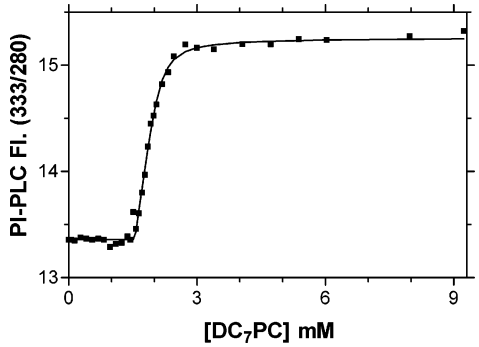

FIGURE 8: Change in the tryptophan-emission intensity of PI-PLC at 333 nm (excitation at 280 nm) with DC_7PC concentration. Note that the signal intensity changes only above the CMC. These results are adequately fitted (line) to eq 8a with a_1 = 0, N = 290, and K_d = 0.76 μM (using K_2 = 0.2 mM and n = 2 from Figures 3 and 5). N is the apparent site exclusion, and K_d is the dissociation constant for enzyme bound to micelles (Appendix, section 1). Note that no change was observed between 3 and 10 mM DC_7PC, which shows that the micellar polymorphs have little effect on the fluorescence intensity and spectrum (not shown).

detailed balance condition of the model (eq 1) that the signal in Figure 8 is predominantly for E* to $E^{\#}$ with dissociation constant $K_d(CMC/K_2)^n$. Thus the effective dissociation constant from E* (to E and $E^{\#}$) is $K_d^{eff} = K_d[1 + (CMC/K_2)^n]$.

In Table 3 are listed both K_d and the effective K_d^{eff} values (to E and $E^{\#}$) for E* bound to PN14 micelles alone and to DC_7PC micelles alone or in the presence of oct-PM, HPM,

Table 3: Effective K_d for PI-PLC Bound to Micelles

amphiphile	additive	K_d (μM)[a]	K_d^{eff} (μM)	N	CMC (μM)
PN14	none		4.4	110	95
DC_7PC	none	0.76	46	290	1550
DC_7PC	1 mM oct-PM	0.45	23	490	1400
DC_7PC	0.01 mM HPM	0.61	26	620	1300
DC_7PC	0.01 mM PN16	0.05	1.3	760	1000

[a] K_d is defined per mole of lipid in micelles. Therefore, K_d corresponds approximately to NK_D in ref *28*, where K_D refers to binding per site of size N on micelles.

and PN16. Like DC_7PC, PN14 and PN16 (*7*) do not have significant affinity for the active site of PI-PLC. HPM and oct-PM bind the catalytic site, and in their presence, the bound enzyme is likely to be in the E*L form (Figure 1). In all of these cases, the overall increase in the signal at 333 nm is about 15%. If the values of n and K_2 do not change in the presence of the additives, the K_d values for the binding of PI-PLC to DC_7PC micelles or comicelles with HPM or oct-PM are not significantly different. Values of N for DC_7PC in the presence of the additives increase about 2-fold. On the other hand, $N = 110$ for PN14 is significantly lower than that with DC_7PC. In contrast to K_d, the estimated values of N and K_d^{eff} in Table 3 do not depend on the assumed values of n and K_2.

It should be noted that the model (Appendix, section 1) used for these parameter estimates (n, K_2, N, K_d) does not take into account the aggregate formation of $E^{\#}$. If such aggregates exist, they would further stabilize the $E^{\#}$ state(s). Thus, ignoring aggregate formation would lead to an underestimate of K_2. For instance, if $E^{\#}$ with DC_7PC alone forms dimers with dissociation constant 0.1 μM, we find (data not shown) from best fits with the data in Figures 3 and 8 $n = 1.6$, $K_2 = 0.65$ mM, $N = 230$, and $K_d = 5.2$ μM ($K_d^{eff} = 35$ μM). If the assumed aggregate stability is decreased, the parameter estimates approach those reported above (Figures 3 and 8). However the goodness of fit did not change, and we have no reliable way of knowing either the stoichiometry or stability of these aggregates. Thus we have chosen to ignore the reality of $E^{\#}$ aggregation, but it should be noted that as defined above the estimated parameter values are apparent if they involve contributions from the aggregation of $E^{\#}$. Such aggregation would be strongly dependent on enzyme concentration. Thus if it contributes significantly, the neglect of aggregation in the analysis would lead to a systematic decrease in the estimated K_2 with increasing enzyme concentration. This was not observed (data not shown) when enzyme concentration was increased from 1 to 2 to 3 μM.

Many of the measurements of interest require mixtures of amphiphiles where the IMC value can be significantly different than the CMC values for the individual amphiphiles (Table 1). In this context, it is important to note that the CMC of DC_7PC, as sensed by the change in the tryptophan emission at 333 nm, does not change in the presence of PI-PLC (Table 3). By this criterion, the onset of micellization occurs at 1.4 mM DC_7PC in the presence of 10 μM HPM or 1 mM oct-PM. On the other hand, the onset of micellization in the presence of 10 μM PN16 is at 1 mM. The change in the tryptophan signal at the CMC of DC_7PC reflects a change in the microenvironment by PI-PLC. Therefore it is of interest to examine the effect of PI-PLC on the CMC and IMC.

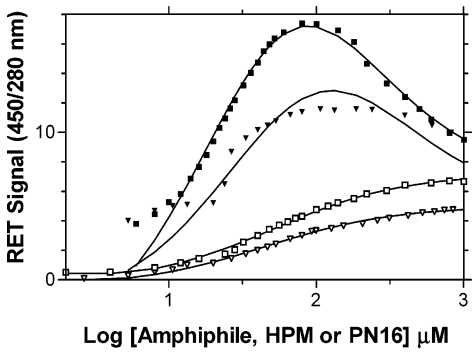

FIGURE 9: Change in the fluorescence emission intensity of a mixture of 1 μM TMA-DPH and 1 mM DC_7PC (unfilled symbols) without or (filled symbols) with 2 μM PI-PLC. The reaction mixture was titrated with (square) HPM or (triangle) PN16. Excitation was at 280 nm with RET emission at 450 nm (with 4 nm slit widths) for all measurements. Best fits with eq 16 are also shown: the best fit parameters for HPM are $K' = 57$ μM, $N = 0$, and $K_d = 72$ μM; those for PN16 are $K' = 55$ μM, $N = 0$, and $K_d = 173$ μM. A significant departure below 10 μM amphiphile could come from the fact that for these comicelles the IMC is 4−5 μM (Table 1). The focus of the model is only for the binding and partitioning to comicelles. Note the logarithmic scale on the x-axis used to separate the low-concentration data points.

PI-PLC Binding to Comicelles of HPM or PN16 with DC_7PC. Onset of (co)micellization was monitored as a change in the emission intensity of NPN, which increases dramatically as it partitions into the micelles. These results (not shown) for the comicellization of HPM or PN16 with DC_7PC are consistent with the results in Table 1. Since the partition coefficient (K') of NPN is about 50 μM, it does not give a significant signal with 2 μM E or $E^{\#}$. With HPM alone, the onset of a significant increase in the signal occurs at 75 μM HPM, which is also the CMC from the surface tension measurements (Table 1). In the presence of 1 mM DC_7PC, onset of the NPN signal shifts to less than 10 μM HPM, which is also consistent with the IMC of 5 μM HPM. Such measurements also showed that the CMC or IMC of HPM does not change significantly in the presence of PI-PLC as is also apparent for DC_7PC alone (Figure 8).

RET from PI-PLC to TMA-DPH in Comicelles. Evidence for binding of PI-PLC to the comicelles was obtained with the RET signal from PI-PLC to TMA-DPH, a cationic derivative of diphenylhexatriene. Its RET distance from tryptophan is about 1 nm. TMA-DPH is not an ideal acceptor because in addition to its main absorbance peak at 355 nm it also has an excitation band at 280 nm. Results with TMA-DPH show that an increase in the RET intensity at 450 nm is accompanied by a decrease in the tryptophan emission at 333 nm. Results in Figure 9 show the partitioning and the RET behavior of TMA-DPH in comicelles with or without PI-PLC. The probe is virtually completely quenched in the aqueous phase. In the absence of the PI-PLC, the hyperbolic curves for the titration of 1 μM TMA-DPH in 1 mM DC_7PC with anionic HPM or zwitterionic PN16 show an increase due to the partitioning of TMA-DPH in the comicelles. The fit for the partitioning equilibrium with PN16 or HPM gives virtually the same value of the partition coefficient K' (section 3 in Appendix). The values in the legend of Figure 9 show that K' for the cationic TMA-DPH is the same for the zwitterionic and anionic comicelles.

As also shown in Figure 9, in the presence of PI-PLC the concentration dependence of the signal is biphasic. We attribute the initial increase to the RET from PI-PLC donor to TMA-DPH acceptor colocalized in comicelles of DC_7PC with HPM or PN16. It peaks near K'. At the higher amphiphile concentrations, the RET signal intensity decreases as E* and probe distribute in separate comicelles. This interpretation is consistent with the changes in the acceptor and donor spectra (results not shown). For example, in the rising phase at lower amphiphile concentrations, the donor (tryptophan) emission decreases with a concurrent increase in the RET signal from the acceptor. In the falling phase above 0.1 mM amphiphile concentration, the direction of both changes reverses until the spectrum of the tryptophan donor from PI-PLC is recovered at about 2 mM PN16 or HPM.

The fits in Figure 9 show that the RET results are in accord with the model that we have considered so far (section 3 in Appendix). According to eq 16, the following changes contribute to the observed behavior. An increasing number of the comicelles provide surface for the partitioning of the probe, for the binding of PI-PLC to the comicelles containing the probe, and finally for the dilution of PI-PLC and the probe into separate micelles. For the fit to eq 16, we assume that K' remains the same with and without the enzyme. Both of the fits in Figure 9 show a systematic departure at low amphiphile concentration and for PN16 also at high amphiphile concentrations. There are several possible explanations that cannot be sorted out yet for the following reason. In its simplest form, the model (section 3 in Appendix) is based on the assumption that the RET signal is related to the binding of PI-PLC to comicelles of HPM or PN16 containing the acceptor. Three possible effects are assumed to be negligible: (a) the effect of the occupancy of the active site; (b) the effect of the enzyme binding on K'; (c) the difference in the surface charge on the RET efficiency. Also note that eq 16 neglects any possible influence from $E^{\#}$, which is likely to be significant at 1 mM DC_7PC with $K_2 = 0.2$ mM. Thus the estimated K_d value actually corresponds to K_d^{eff}. The model also ignores changes in binding (K_d) and partitioning (K') due to changes in composition of the comicelles with increasing amount of added HPM or PN16. The comicellar interface here is different than that in Figure 8 or Table 3, and therefore, the K_d values are not comparable. At this stage, it is not possible to quantitatively analyze all of these effects, and the fits in Figure 9 are intended primarily to show that despite such approximations results are in reasonable accord with the model.

DISCUSSION

A rationale for a role of phosphatidylcholine in the regulation of bacterial PI-PLC comes from the fact that its physiological target is mammalian cell membranes where PI at low mole fraction is codispersed in the plasma membrane rich in phosphatidylcholine (*24*). Our results on the binding of monodisperse DC_7PC to PI-PLC are interpreted in terms of the model of interactions along the i-face of PI-PLC (Figure 1). Although in qualitative accord, our results and interpretation differ from those proposed for the dependence of the ^{31}P NMR line-width resulting from the exchange of DC_7PC bound to PI-PLC (*25*) or the kinetic results with a monodisperse substrate (*18*, *19*). These latter results were interpreted with the assumption that one or two molecules of monodispersed DC_7PC bind to PI-PLC. While these results are not inconsistent with eq 1 (Appendix), our results clearly show that the $E^{\#}$ species formed with monodispersed DC_7PC is more complex than a simple EA or EA_2 complex postulated before.

Our results show that $E^{\#}$ formed with monodisperse DC_7PC is different than E* formed with micelles. The behavior of $E^{\#}$ suggests that it self-aggregates (Table 2) and partitions hydrophobic probes (Figures 6, 7, and 9). We believe that the formation of $E^{\#}$ type of species is likely to be the first step in any interfacial kinetic path where monodisperse amphiphiles including the substrate and inhibitors are present. A quantitative understanding of the underlying microscopic event(s) is therefore critical for understanding the behaviors of PI-PLC at interfaces. Since the coupling between the interface binding and the turnover events is the crux of interfacial enzyme kinetics (*1*), consider the functional consequence of E, $E^{\#}$, and E* (Figure 1A−C) in relation to the interfacial kinetic paradigm (*1*, *5*): (a) Binding of substrate to PI-PLC in E, $E^{\#}$, and E* could lead to at least three distinct kinetic paths, each with its unique environment for the microscopic steady state. The number of possible kinetic paths would increase dramatically if the residence time of the enzyme in the $E^{\#}$ and E* is of the order of the catalytic turnover time with low interfacial turnover processivity. (b) Allosteric activation by amphiphile(s) could change the Michaelis−Menten kinetic parameters for E, $E^{\#}$, and E*. Available evidence suggests that full interfacial activation of PI-PLC is also seen at the PI interface with bile salts in the absence of phosphatidylcholine (*7*). (c) Distribution of total enzyme in each of the states is influenced not only by the amphiphile concentration but also by the propensity of $E^{\#}$ and E* to undergo additional changes; for example, the aggregation of $E^{\#}$ or the binding of the active site directed ligands (L).

Structural functional analysis for enzymes can only be carried out in terms of the primary events. Starting with the interfacial kinetic paradigm (Figure 1), a kinetic model can be analyzed only if the turnover path is unequivocally established and all alternative paths are ruled out. Considerations outlined above emphasize the challenge of designing assays. None of the available equilibrium and kinetic assays with PI-PLC can be adequately analyzed at this stage in terms of the primary events because the underlying assumptions are not established. With a focus on the initial events that must precede any catalytic turnover path(s), in the following discussion we elaborate on the implicit and explicit assumptions necessary for the analysis of the primary events in eq 1 (Appendix).

Significance of the Hill Coefficient. From the properties of $E^{\#}$, it is apparent that it contains several DC_7PC molecules per PI-PLC, which we believe to be bound along the i-face of the enzyme (Figure 1A and eq 1). In the context of the equilibria with amphiphiles (*1*), for the discussion below, it is worth considering the significance of the fit parameters. Binding of E to a preformed interface (A*) without any soluble A is treated as a single E to E* step. $E^{\#}$ is formed in the presence of monodisperse A. According to eq 1, K_d is defined for the dissociation of E* to E; however, by detailed balance, the stability of E* will also have a contribution from

$E^{\#}$. K' is the dissociation constant for a probe in micelles. Not only the CMC, the dissociation constant for a monomer amphiphile from a micelle, is clearly different from K_d or K_2, the difference also holds for n and N, neither of which is the same as the micellar aggregation number. In effect, the difference shows that the stability and dynamics of DC_7PC in micelles is significantly different than in $E^{\#}$ or E*.

The dissociation constant for monodisperse DC_7PC from $E^{\#}$ is $K_2 = 0.2$ mM with Hill coefficient $n = 2$. Since the CMC is 1.5 mM, the stability of DC_7PC in $E^{\#}$ is about 7.5-fold better than it is in its micelles. If the repulsive interactions between the polar headgroup of DC_7PC in $E^{\#}$ are reduced by desolvation or the charge compensation with the residues on the i-face, DC_7PC would have a more pronounced tendency to aggregate along the i-face. Assuming that there is an all-or-nothing binding, the Hill coefficient describes the apparent number of the cooperative sites involved in the formation of $E^{\#}$. If the formation of $E^{\#}$ is a multistep process, n could also be the number of amphiphiles bound in the initial step or an effective number for the binding of more than two amphiphiles. For example, if 20 molecules bind with less than total cooperativity, this means that there could be contributions from intermediate binding states with or without an allosteric change in PI-PLC.

Size-exclusion chromatography suggests that the PI-PLC concentration in the eluted high molecular weight complex peak is 0.1 μM PI-PLC although the injected enzyme concentration is 15 μM. Self-aggregation of $E^{\#}$ could also influence the interpretation of K_2 and introduce a dependence on enzyme concentration. Comparable values of K_2 are obtained in the fluorescence (Figure 5) and calorimetric (Figure 3) measurements carried out at similar (1−3 μM PI-PLC) concentrations. The lack of enzyme-concentration dependence in the estimate of K_2 suggests that an effective dissociation constant for $E^{\#}$ aggregation would be around 1 μM or larger. If aggregation of $E^{\#}$ contributes significantly, neglecting it in the analysis would lead to overestimates of n and underestimates of K_2. The reported value of $K_2 = 0.3$ mM from the TRNOE measurements at ca. 50 μM PI-PLC (*25*) also suggests that the effect of aggregation on the estimate of K_2 may be insignificant.

*Dissociation Equilibrium for E**. Within available considerations, binding of PI-PLC to DC_7PC micelles is analyzed in a two-parameter model with an apparent site-exclusion parameter N and the dissociation constant K_d (eq 6). The estimated N-values in many cases seem much too large to correspond to the number of amphiphiles "covered" by one enzyme or the size of DC_7PC micelle. Partially it would represent the stoichiometry in the enzyme−micelle complex, but also other effects, for example, aggregation, not included in the model could affect the estimate of N.

K_d is defined as the dissociation constant from E* on the micelle to E. However, at least for DC_7PC, we know that at the onset of micellization E is present as $E^{\#}$. Consequently, the binding curve monitors the dissociation of E* to $E^{\#}$, although the signal at 333 nm is indistinguishable for E and $E^{\#}$. In this case, a true K_d for E* to E cannot be deduced without accounting for the influence of $E^{\#}$ (through K_2 and n). The effective dissociation (Table 3) from E* (to E and $E^{\#}$) consequently has a contribution also from the properties of $E^{\#}$ according to eq 1 (Appendix) and detailed balance. Also note that K_d is defined per mole of lipid in micelles and therefore corresponds approximately to NK_D (see footnote to Table 3) as defined in an earlier analysis (*28*).

Monomer Kinetics and Interfacial Activation. Kinetic interpretation of the hydrolysis of monodisperse substrates by interfacial enzyme is not trivial. For example, the turnover path for the phospholipase A_2 (*26*) and lipase (*27*) catalyzed hydrolysis of monodisperse substrates is on the extraneous surfaces such as the vessel walls and the air bubbles. For an appreciation of another competing or alternate kinetic path, consider the difficulties inherent in the kinetic interpretation of the PI-PLC-catalyzed hydrolysis of monodisperse substrate. Apparently the observed monomer hydrolysis does not occur on the vessel walls (*18*, *19*). This has been interpreted to suggest that the turnover occurs through a classical Michaelis−Menten complex of PI-PLC that is allosterically activated by the binding of one (*25*) or two (*18*, *19*) molecules of monodispersed phosphatidylcholine. Based on the properties of $E^{\#}$ formed with monodispersed DC_7PC, our interpretation is that the activation of the PI-PLC catalyzed turnover of the "soluble" substrate could occur through an $E^{\#}S$ type of Michaelis complex. This interpretation is consistent not only with the Hill coefficient of 2 in the binding of phosphocholine but also with the fact that the aggregate of such a premicellar complex would remain in the bulk aqueous phase rather than adsorb on the extraneous surfaces. Kinetic and structural consequences of this suggestion remain to be fully explored.

ACKNOWLEDGMENT

We thank Professor Mary Roberts for providing us the key TRNOE results from their earlier publication (*25*). We gratefully acknowledge useful insights provided by Professor Tatyana Polenova into the significance of these results.

APPENDIX

Models

1. Enzyme−Amphiphile Binding. The results in this paper show that PI-PLC can bind amphiphile in at least two different ways, a premicellar complex $E^{\#}$ or E* at preformed micelles. This suggests the following reaction scheme:

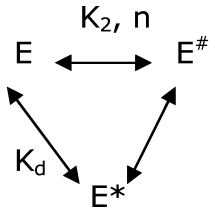

(1)

The equilibrium constant between $E^{\#}$ and E* is determined by detailed balance from the other two equilibria in this scheme. The premicellar complex, $E^{\#}$, is assumed to form cooperatively with Hill parameter n and dissociation constant K_2. At equilibrium, this gives the concentration of complexes:

$$[E^{\#}] = E_f(c_f/K_2)^n \quad (2)$$

$$[E^*] = E_f m_f/K_d \quad (3)$$

E_f is the concentration of free enzyme, and c_f is the

concentration of free amphiphile that is monodisperse in solution:

$$c_f = \begin{cases} c; & \text{if } c < \text{CMC} \\ \text{CMC}; & \text{if } c \geq \text{CMC} \end{cases} \quad (4)$$

where c is the total concentration of added amphiphile. m_f is the concentration of micellar amphiphile that is available for binding of E:

$$m_f = c - \text{CMC} - N[\text{E}^*] = c - \text{CMC} - NE_f m_f/K_d; \quad \text{if } c > \text{CMC} \quad (5a)$$

Thus,

$$m_f = \begin{cases} 0; & c \leq \text{CMC} \\ \dfrac{c - \text{CMC}}{1 + NE_f/K_d}; & c > CMC \end{cases} \quad (5b)$$

N is a site-exclusion parameter that accounts for the number of micellar amphiphiles that are "covered" by each bound enzyme and not available for binding further enzymes (*28*). It is to be considered a fitting parameter that may also account for other effects, for example, higher-complex formation, etc. In this formulation, it is assumed that amphiphile is in excess, $c \gg [\text{E}]$, so that the concentration of amphiphiles that are bound in the $\text{E}^{\#}$ complexes can be neglected relative to c. When this is not the case, c_f needs to be calculated; cf. eq 11 below.

This gives the total concentration of enzyme:

$$E_T = E_f\left\{1 + \left(\frac{c_f}{K_2}\right)^n + \frac{c - \text{CMC}}{K_d + NE_f}\right\} \quad (6)$$

The last term in eq 6 comes from eq 5b and contributes only when $c >$CMC. E_f can be solved from eq 6 giving

$$E_f(c) = -\frac{1}{2N}\left\{K_d + \frac{c - \text{CMC} - NE_T}{1 + (c_f(c)/K_2)^n}\right\} + \frac{1}{2N}\sqrt{\{...\}^2 + \frac{4K_d NE_T}{1 + (c_f(c)/K_2)^n}} \quad (7)$$

The term in curly brackets under the root sign is the same as the one outside. Assuming that $\text{E}^{\#}$ and E* give signal a_1 and a_2, respectively, the total signal after titration to concentration c of the amphiphile is

$$S(c) = E_f(c)\left(a_1\left(\frac{c_f(c)}{K_2}\right)^n + a_2\frac{c - \text{CMC}}{K_d + NE_f(c)}\right) \quad (8a)$$

Above the CMC, $c_f = \text{CMC}$. Below the CMC, the term $c -$ CMC is zero and $c_f = c$ in the equations above, and the result reduces to the Hill equation:

$$S(c) = a_1\frac{(c/K_2)^n E_T}{1 + (c/K_2)^n} \quad (8b)$$

2. Two-State Binding below CMC. The binding of HDNS to the enzyme (Figure 7) suggests that this binding below CMC can take place in at least two different ways:

$$\text{E1} \overset{K_1}{\leftrightarrow} \text{E} \overset{n, K_2}{\leftrightarrow} \text{E}^{\#} \quad (9)$$

The first state, E1, is the binding of a single amphihile to a specific site, not necessarily the catalytic site, with dissociation constant K_1, and the second state is a cooperative binding of N_2 amphiphiles with Hill parameters n and K_2. The concentration of free enzyme is given by

$$E_f = \frac{E_T}{1 + c_f/K_1 + (c_f/K_2)^n} \quad (10)$$

The concentration, c_f, of free amhiphiles can be solved numerically from

$$c = c_f + E_f(c_f/K_1) + E_f N_2(c_f/K_2)^n \quad (11)$$

Assuming that the amphiphile has signal a_1 when bound singly in state E1 and a_2 when bound in the complex $\text{E}^{\#}$, the total signal can be expressed as

$$S(E_T,c) = a_1\frac{E_f c_f}{K_1} + a_2 N_2 E_f\left(\frac{c_f}{K_2}\right)^n \quad (12)$$

The results of this two-state binding, eq 9, are indistinguishable from a model where binding is consecutive, E ↔ E1 ↔ E#; only n and K_2 will be reinterpreted.

3. Probe Binding and Partitioning above CMC. Consider the situation where enzyme and a probe are in a solution that is titrated with an amphiphile at concentration c. The probe P is assumed to partition into micelles with dissociation constant K'. If the total concentration of probe is P_T, the concentration, P_b, of probe bound in micelles is

$$P_b = \frac{(c - \text{CMC})P_T}{c - \text{CMC} + K'} \quad (13)$$

Assuming that binding of enzyme and partitioning of the probe are independent, the concentration of enzyme bound to micelles is (cf. eq 7)

$$E_b(c) = \frac{1}{2N}\{c - \text{CMC} + K_d + NE_T\} - \frac{1}{2N}\sqrt{\{...\}^2 - 4NE_T(c - \text{CMC})} \quad (14)$$

The term inside curly brackets under the root sign is the same as the one outside. If N_M is the size of a micelle and each micelle binds only one enzyme, the fraction of micelles with an enzyme bound is

$$f_b = \frac{N_M E_b}{c - \text{CMC}} \quad (15)$$

f_b also corresponds to the probability that a bound probe is in a micelle that carries an enzyme. N_M in this expression may be better viewed as the number of micellar amphiphiles associated with each bound enzyme. Possibly $N_M = N$. If the probe in a micelle with enzyme has signal a_1 and without enzyme has signal a_2, the total signal as a function of the concentration, c, of added amphiphile is

$$S(c) = P_b[a_1 f_b + a_2(1 - f_b)] = \frac{P_T(c - \mathrm{CMC})}{c - \mathrm{CMC} + K'}\left[a_2 + (a_1 - a_2)\frac{N_M E_b(c)}{c - \mathrm{CMC}}\right] \quad (16)$$

This result is valid only for $c > \mathrm{CMC}$ and neglects contributions from the binding of probe to enzyme in premicellar states.

Thus a_2 and K' are determined from the best fit of eq 16 with the results in the absence of E, that is, for $E_b = 0$. Note that the a_2 values for the two comicelles in Figure 9 are noticeably different, while the K' values are the same. There remain three parameters, K_d, N, and a_1, to be determined from the fits with the results in the presence of enzyme. The estimated values of K_d and the apparent site exclusion, N, in the model do not depend on the value used for micelle size (N_M). Also the observed value of N relates only to the changing concentration of the titrant, whereas the signal comes from the enzyme bound to the comicelles with DC_7PC.

REFERENCES

1. Berg, O. G., and Jain, M. K. (2001) *Interfacial Enzyme Kinetics*, p 302, John Wiley & Sons, Chichester, U.K.
2. Verheij, H. M., Slotboom, A. J., and de Haas, G. H. (1981) Structure and Function of Phospholipase A2, *Rev. Physiol. Biochem. Pharmacol. 91*, 91−203.
3. Jain, M. K., and Berg, O. G. (1989) Kinetics of interfacial catalysis by phospholipase A_2 and regulation of interfacial activation and inhibition, *Biochim. Biophys. Acta 1002*, 127−156.
4. Ramirez, F., and Jain, M. K. (1991) Phospholipase A2 at the bilayer interface, *Proteins 9*, 229−239.
5. Berg, O. G., Tsai, M. D., Gelb, M. H., and Jain, M. K. (2001) Interfacial Enzymology: The secreted phospholipase A_2-paradigm, *Chem. Rev. 101*, 2613−2653.
6. Yu, B. Z., Apitz-Castro, R., Tsai, M. D., and Jain, M. K. (2003) Interaction of monodisperse anionic amphiphiles with the i-face of secreted phospholipase A_2, *Biochemistry 42*, 6293−6301.
7. Volwerk, J. J., Filthuth, E., Griffith, O. H., and Jain, M. K. (1994) Phosphoinositol-specific phospholipase C from *Bacillus cereus* at the lipid-water interface: Interfacial binding, catalysis and activation, *Biochemistry 33*, 3464−3474.
8. Griffith, O. H., and Ryan, M. (1999) Bacterial phosphatidylinositol-specific phospholipase C: structure, function, and interaction with lipids, *Biochim. Biophys. Acta 1441*, 237−254.
9. Lewis, K. A., Garigapati, V. R., Zhou, C., and Roberts, M. F. (1993) Substrate requirements of bacterial phosphatidylinositol-specific phospholipase C, *Biochemistry 32*, 8836−8841.
10. Heinz, D. W., Ryan, M., Smith, M. P., Weaver, L. H., Keana, J. F., and Griffith, O. H. (1996) Crystal structure of phosphatidylinositol-specific phospholipase C from *Bacillus cereus* in complex with glucosaminyl(α1→6)-D-*myo*-inositol, an essential fragment of GPI anchors, *Biochemistry 35*, 9496−9504.
11. Gassler, C. S., Ryan, M., Liu, T., Griffith, O. H., and Heinz, D. W. (1997) Probing the roles of active site residues in phosphatidylinositol-specific phospholipase C from *Bacillus cereus* by site-directed mutagenesis, *Biochemistry 36*, 12802.
12. Feng, J., Wehbi, H., and Roberts, M. F. (2002) Role of tryptophan residues in interfacial binding of phosphatidylinositol-specific phospholipase C, *J. Biol. Chem. 277*, 19867−19875.
13. Feng, J., Bradley, W. D., and Roberts, M. F. (2003) Optimizing the interfacial binding and activity of a bacterial phosphatidylinositol-specific phospholipase C, *J. Biol. Chem. 278*, 24651−24657.
14. Quian, X., Zhou, C., and Roberts, M. F. (1998) Phosphatidylcholine activation of bacterial phosphatidylinositol-specific phospholipase C toward PI vesicles, *Biochemistry 37*, 6513−6522.
15. Zhou C, Wu Y, and Roberts, M. F. (1997) Activation of phosphatidylinositol-specific phospholipase C toward inositol 1,2-(cyclic)-phosphate, *Biochemistry 36*, 347−355.
16. Hendrickson, H. S., Hendrickson, E. K., Johnson, J. L., Khan, T. H., and Chial, H. J. (1992) Kinetics of *Bacillus cereus* phosphatidylinositol-specific phospholipase C with thiophosphate and fluorescent analogues of phosphatidylinositol, *Biochemistry 31*, 12169−12172.
17. Zhou, C., and Roberts, M. F. (1998) Nonessential activation and competitive inhibition of bacterial phosphatidylinositol-specific phospholipase C by short-chain phospholipids and analogues, *Biochemistry 37*, 16430−16439.
18. Ryan, M., Zaikova, T. O., Keana, J. F. W., Goldfine, H., and Griffith, O. H. (2002) *Listeria monocytogenes* phosphatidylinositol-specific phospholipase C: activation and allostery, *Biophys. Chem. 101−102*, 347−358.
19. Birrell, G. B., Zaikova, T. O., Rukavishnikov, A. V., Keana, J. F., and Griffith, O. H. (2003) Allosteric interactions within subsites of a monomeric enzyme: Kinetics of fluorogenic substrates of PI-specific phospholipase C, *Biophys. J. 84*, 3264−3275.
20. Jain, M. K., and Vaz, W. L. C. (1987) Dehydration of the lipid-protein microinterface on binding of phospholipase A_2 to lipid bilayers, *Biochim. Biophys. Acta 905*, 1−8.
21. Lin, T. L., Chen, S. H., Gabirel, N. E., and Roberts, M. F. (1987) Small-angle neutron scattering techniques applied to the study of polydisperse rodlike diheptanoylphosphatidylcholine micelles, *J. Phys. Chem. 91*, 406−409.
22. Goldfine, H., and Knob, C. (1992) Purification and characterization of *Listeria monocytogenes* phosphatidylinositol-specific phospholipase C, *Infect. Immun. 60*, 4059−4067.
23. Ellis, M. V., James, S. R., Parisic, O., Downes, C. P., Williams, R. L., and Katan, M. (1998) Catalytic domain of phosphoinositide-specific phospholipase C (PLC). Mutational analysis of residues within the active site and hydrophobic ridge of plcdelta1, *J. Biol. Chem. 273*, 11650−11659.
24. Wadsworth, S. J., and Goldfine, H. (2002) Mobilization of protein kinase C in macrophages induced by *Listeria monocytogenes* affects its internalization and escape from the phagosome, *Infect. Immun. 70*, 4650−4660.
25. Zhou, C., Qian, X., and Roberts, M. F. (1997) Allosteric activation of phosphatidylinositol-specific phospholipase C: specific phospholipid binding anchors the enzyme to the interface, *Biochemistry 36*, 10089−10097.
26. Yu, B. Z., Berg, O. G., and Jain, M. K. (1999) Hydrolysis of monodisperse substrate by phospholipase A_2 occurs at vessel walls and air bubbles, *Biochemistry 38*, 10449−10456.
27. Berg, O. G., Cajal, Y., Butterfoss, G. L., Grey, R. L., Alsina, M. A., Yu, B. Z., and Jain, M. K. (1998) Interfacial activation of triglyceride lipase from *Thermomyces (Humicola) lanuginosa*: kinetic parameters and a basis for control of the lid, *Biochemistry 37*, 6615−6627.
28. Hille, J. D. R., Den Kelder, G. M., Sauve, P., De Haas, G. H., and Egmond, M. R. (1981) Physicochemical studies on the interaction of pancreatic phospholipase A_2 with micellar substrate analogue, *Biochemistry 20*, 4068−4073.

BI035063J